Title
Targeting H3K4 trimethylation in Huntington disease

Journal
Proceedings of the National Academy of Sciences of the United States of America, 110(32)

ISSN
0027-8424

Authors
Vashishtha, Malini
Ng, Christopher W
Yildirim, Ferah
et al.

Publication Date
2013-08-06

DOI
10.1073/pnas.1311323110

Targeting H3K4 trimethylation in Huntington disease

Malini Vashishtha[a,1], Christopher W. Ng[b,1], Ferah Yildirim[b,1], Theresa A. Gipson[c], Ian H. Kratter[d], Laszlo Bodai[e], Wan Song[e], Alice Lau[a], Adam Labadorf[b], Annie Vogel-Ciernia[f], Juan Troncosco[g], Christopher A. Ross[g], Gillian P. Bates[h], Dimitri Krainc[i], Ghazaleh Sadri-Vakili[i], Steven Finkbeiner[j], J. Lawrence Marsh[e], David E. Housman[c,2], Ernest Fraenkel[b,2], and Leslie M. Thompson[a,f,2]

[a]Department of Psychiatry and Human Behavior and UCI Institute of Memory Impairments and Neurological Disorders, [e]Department of Developmental and Cell Biology and Developmental Biology Center, and [f]Department of Neurobiology and Behavior, University of California, Irvine, CA 92697; [b]Department of Biological Engineering and [c]Center for Cancer Research, Massachusetts Institute of Technology, Cambridge, MA 02139; [d]Gladstone Institute of Neurological Disease Biomedical Sciences Graduate Program and Medical Scientist Training Program and [j]Gladstone Institute of Neurological Disease Taube-Koret Center for Huntington's Disease Research, Departments of Neurology and Physiology, University of California, San Francisco, CA 94158; [g]Departments of Psychiatry, Neurology, and Neuroscience and Neuropathology, Johns Hopkins University, Baltimore, MD 21287; [h]Department of Medical and Molecular Genetics, King's College, London SE1 9RT, United Kingdom; and [i]Department of Neurology, Massachusetts General Hospital, Boston, MA 02114

Contributed by David E. Housman, June 18, 2013 (sent for review May 7, 2013)

Transcriptional dysregulation is an early feature of Huntington disease (HD). We observed gene-specific changes in histone H3 lysine 4 trimethylation (H3K4me3) at transcriptionally repressed promoters in R6/2 mouse and human HD brain. Genome-wide analysis showed a chromatin signature for this mark. Reducing the levels of the H3K4 demethylase *SMCX/Jarid1c* in primary neurons reversed down-regulation of key neuronal genes caused by mutant Huntingtin expression. Finally, reduction of *SMCX/Jarid1c* in primary neurons from BACHD mice or the single *Jarid1* in a *Drosophila* HD model was protective. Therefore, targeting this epigenetic signature may be an effective strategy to ameliorate the consequences of HD.

polyglutamine | neurodegeneration

Huntington disease (HD), a neurodegenerative disease (1, 2) characterized by cognitive dysfunction, psychiatric symptoms, and choreic movements (2), exhibits brain region-specific neuronal degeneration in the striatum and cortex. Currently, no disease-modifying treatment is available. The genetic basis of HD is the expansion of an in-frame CAG repeat sequence encoding polyglutamine. Progressive transcriptional dysregulation in both cortex and striatum and atrophy of the cortex are characteristic features (3). Transcriptional repression of key neuronal transcripts, including neurotransmitters, growth factors, and their cognate receptors, is consistently observed and implicated in disease pathogenesis. Among the critical genes whose expression is repressed in HD mouse models and human brain tissue are the dopamine receptor 2 (*Drd2*), preproenkephalin (*Penk1*), the cannabinoid receptor (*Cb2*), and brain-derived neurotrophic factor (*Bdnf*) (4, 5).

We hypothesized that a central event in the pathological program underlying transcriptional dysregulation includes alterations in chromatin structure in the regulatory regions of genes down-regulated in HD. To evaluate this hypothesis, we focused on H3K4 trimethylation (H3K4me3), a mark of transcription start sites (TSSs) and active chromatin (6–8). Growing evidence suggests that this mark is plastic and modulated in conditions of chronic stress, developmental disorders, psychiatric disorders (9–11) as well as during long-term memory consolidation from contextual fear conditioning (12), suggesting a critical function in brain.

We first investigated H3K4me3 in the R6/2 mouse model of HD, which shows patterns of transcriptional dysregulation similar to postmortem HD brain (13, 14). Using chromatin immunoprecipitation (ChIP), we examined H3K4me3 levels for *Bdnf*, which is expressed in the cortex, provides trophic support for GABAergic medium spiny neurons, and is expressed at lower levels in HD (5, 15). The potential significance of *Bdnf* in HD is reflected by transcriptional profiling (16) and therapeutic preclinical studies (17, 18). Because H3K4me3 levels were lowered at *Bdnf* and other promoters in R6/2 mice and key neuronal genes in human HD brain cortex and striata, we expanded our approach to investigate the genome-wide relationship between H3K4me3 and sites of transcriptional dysregulation in HD model mice. We, indeed, observed strong correlations between H3K4me3 levels and changes in relative transcription levels.

Through these studies, we discovered a striking chromatin signature that identifies a specific H3K4me3 chromatin organization pattern at promoters in normal animals that predicts with high likelihood that a promoter will be transcriptionally down-regulated in HD model animals. This pattern is characterized by a broad peak of trimethylation stretching downstream of the TSS. These results suggest that HD targets have a distinct regulatory mechanism in WT mice that is altered, directly or indirectly, by expanded repeat Huntingtin (HTT) and that regulators of chromatin configuration in general and H3K4me3 specifically may play a critical role in the pathway leading to transcriptional dysregulation in HD.

Based on these data, we have taken initial steps to test the hypothesis that treatments altering the distribution of H3K4me3 at these key promoters may be effective in ameliorating the pathological consequences of HD. We tested the impact of re-

Significance

Transcriptional dysregulation is an early and reproducible feature of Huntington disease (HD); however, mechanisms underlying this dysregulation are unclear. This article describes a unique pattern of the chromatin mark H3K4me3 at transcriptionally repressed promoters in HD mouse and human brain identified by genome-wide analysis. Reducing the levels of the demethylase *SMCX/Jarid1c* in primary neurons reversed down-regulation of key neuronal genes caused by mutant Huntingtin expression and was neuroprotective in a *Drosophila* HD model. These results suggest that targeting epigenetic signatures may be an effective strategy to ameliorate the consequences of HD and other neurodegenerative diseases.

Author contributions: M.V., C.W.N., F.Y., T.A.G., I.H.K., A. Lau, S.F., J.L.M., D.E.H., E.F., and L.M.T. designed research; M.V., C.W.N., F.Y., T.A.G., I.H.K., L.B., W.S., A. Lau, A. Labadorf, and A.V.-C. performed research; M.V., C.W.N., F.Y., A. Lau, J.T., C.A.R., G.P.B., D.K., G.S.-V., D.E.H., and E.F. contributed new reagents/analytic tools; M.V., C.W.N., F.Y., T.A.G., I.H.K., L.B., W.S., A. Lau, A. Labadorf, S.F., J.L.M., D.E.H., E.F., and L.M.T. analyzed data; and M.V., C.W.N., F.Y., T.A.G., I.H.K., W.S., G.P.B., S.F., J.L.M., D.E.H., E.F., and L.M.T. wrote the paper.

The authors declare no conflict of interest.

Data deposition: The RNAseq and ChIPseq data reported in this paper have been deposited in the Gene Expression Omnibus (GEO) database, www.ncbi.nlm.nih.gov/geo (accession nos. GSE48960, GSE48962, and GSE48963).

[1]M.V., C.W.N., and F.Y. contributed equally to this work.

[2]To whom correspondence may be addressed. E-mail: dhousman@mit.edu, fraenkel-admin@mit.edu, or lmthomps@uci.edu.

This article contains supporting information online at www.pnas.org/lookup/suppl/doi:10.1073/pnas.1311323110/-/DCSupplemental.

ducing expression of an H3K4me3 demethylase, *Jarid1c*, in cell-based assays and the single H3K4me3 demethylase, *lid*, in a whole-organism model of HD. In these proof-of-concept studies, we show that such reductions restore expression of key down-regulated genes and are protective in cultured primary neurons derived from HD model mice as well as a *Drosophila* model of HD.

Results

H3K4 Trimethylation Changes at the Dysregulated Promoters in HD Model Mice and Human HD Brain. Initial experiments focused on H3K4 methylation levels at the *Bdnf* locus in the R6/2 mouse (19). The mouse *Bdnf* gene has eight 5′ exons that each contain a separate promoter and one 3′ exon coding for the mature protein (Fig. 1*A*) (20). Transcription from both exon II and IV is reduced in cortex from R6/2 mice as well as in human HD brain (21). To examine if *Bdnf* expression correlated with H3K4me3 occupancy, ChIP was used to quantify H3K4me3 at *Bdnf* promoters II–IV and the coding region (IX) in cortices from 12-wk-old R6/2 mice and littermate controls (19). This mouse model, which expresses an expanded repeat-containing fragment of HTT, was selected based on published similarities in gene expression to human HD brain (14). H3K4me3 was reduced by nearly one-half at the RE-1 silencing transcription factor/neuron-restrictive silencer factor (REST/NRSF) promoter II (Fig. 1*B*), suggesting that reduced transcription could be a consequence of changes in chromatin structure at the *Bdnf* locus, specifically a reduction in H3K4me3. This mark was nearly absent upstream of the REST binding site in promoter II and within the coding exon of the *Bdnf* gene (Fig. 1*C*), consistent with other reports (6, 7). Reduction in H3K4me3 occupancy at exon II was observed during symptomatic stages of disease at 8 and 12 wk but not in presymptomatic 4-wk-old mice (Fig. 1 *B* and *D*). Similar results were obtained for cortical and striatal *Penk1* and striatal *Drd2* loci (Fig. 1 *E* and *F*). In contrast, genes with expression levels that are unchanged, such as *Atp5b*, *Rpl13a*, and *Lin7c*, are not altered in H3K4me3 levels (Fig. 1*E*). Western blots confirmed that the changes in H3K4me3 were gene-specific and not the result of a change in bulk H3K4me3 levels in cortices or striata (Fig. S1 *A–D*). The H3K4me3 mark is specifically decreased at the down-regulated genes that we tested. For example, we saw no disease-specific differences in the levels of H3K36me3 occupancy, which also marks actively transcribed genes, within the coding regions of *Bdnf* and *Penk1* in the cortex or *Penk1* and *Drd2* in the striatum (Fig. S1 *E* and *F*).

We next extended our studies of H3K4me3 occupancy to human HD brain. Consistent with previous reports (3, 19), levels of *BDNF* and *SYNAPTOPHYSIN* (*SYP*) in the superior frontal gyrus (SFG) and *DRD2* and *PENK1* in the caudate were significantly lower in the grade 3 samples. In grade 2 samples, there was a trend to decreased expression; however, the difference was not significant (Fig. 2 *A* and *B*). Expression of a control gene

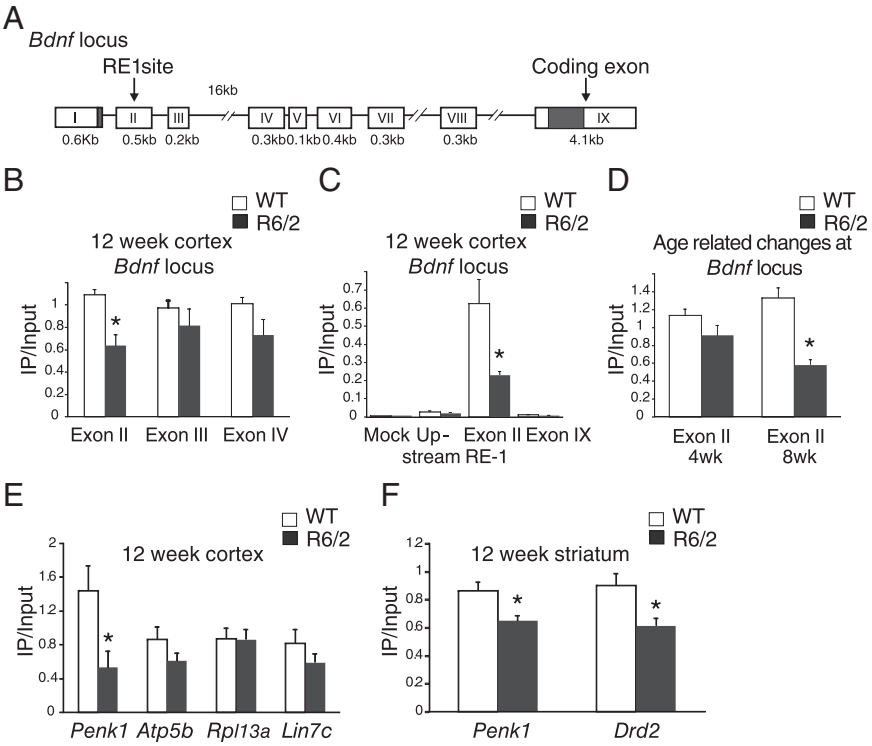

Fig. 1. Levels of H3K4me3 are lower at down-regulated genes in 12-wk-old R6/2 mouse cortex and striatum. (*A*) Schematic view of the mouse *Bdnf* locus. Transcription is alternately initiated at one of several upstream exons. Exon IX contains the coding region of the *Bdnf* gene. Exon II has the NRSF binding site. Exon II of *Bdnf* has a transcriptional repressor REST binding site, whereas CaM kinase II and MAPK kinase can up-regulate exon IV transcription through C/EBPβ and Sp1 transcription factors (21, 55). (*B*) ChIP shows that level of H3K4me3 measured at the exon II locus is nearly one-half of the WT levels, and the difference is significant in 12-wk-old mouse cortex ($P < 0.006$ by one-way ANOVA; $n = 5$). H3K4me3 levels are lower at exons III and IV as well; however, the difference was not significant. (*C*) H3K4me3 levels are specific to TSSs and nearly absent at a region upstream of the TSS by 17,392 bp and at the coding region. No antibody was added in the mock samples. (*D*) Age-related changes in H3K4me3 levels at the exon II start site. At 4 wk, the levels of H3K4me3 at exon II were not different between WT and R6/2 mice, whereas at 8 wk, they were lower in R6/2 mice; the difference was significant. (*E*) H3K4me3 levels were significantly lower at the transcriptional start site of *Penk1* gene in 12-wk-old R6/2 mouse cortex compared with WT mouse ($P < 0.05$ by one-way ANOVA; $n = 4$). At the transcriptional start sites of genes *Atp5b* and *Rpl13a*, the levels of H3K4me3 were similar or lower. However, the difference was not significant. Similar results were found at the *Lin7c* locus, which is downstream of the *Bdnf* locus. (*F*) In 12-wk-old striatum, the levels of H3K4me3 were lower at the transcriptional start site of *Drd2* and *Penk1* loci ($P < 0.05$) by one-way ANOVA ($n = 8$). *$P < 0.05$.

ATP5B was not significantly altered as expected (Fig. 2 *A* and *B*). In these same samples, H3K4me3 occupancy was significantly lower at *BDNF* exon II and *PENK1* and *SYP* promoters but unaltered at *BDNF* exon IV and the *ATP5B* promoter in the SFG grade 3 samples (Fig. 2*C*). For caudate, H3K4me3 levels were lower at *DRD2*, *PENK1*, and *SYP* promoters in grade 2 samples and reduced even further at *Drd2* and *PENK1* promoters in grade 3 samples, potentially preceding corresponding gene expression alterations (Fig. 2*D*). To test if these decreases are specific for H3K4me3 or simply a consequence of decreased expression and/or loss of neuronal tissue, H3K36me3 was evaluated at the coding exon of *BDNF* (*BDNF* IX) where the mark is located and the *DRD2* coding region in caudate. In contrast to H3K4me3, there were no statistically significant decreases in occupancy (Fig. 2 *C* and *D*). Notably, there were also no changes in occupancy of H3K4me3 at *BDNF* exon IV promoter in SFG (Fig. 2*C*). Taken together, these results show that the reduction of H3K4me3 occupancy occurs at down-regulated genes in human HD brain, and this reduction seems selective.

***Bdnf* Promoter Occupancy Is Reduced at TSS in R6/2 Mouse Cortex by ChIP-Seq.** The findings described above prompted us to examine H3K4me3 occupancy across the genome in R6/2 and WT mice at 8 and 12 wk of age for both the cortex and striatum using ChIP-sequencing (Seq) (Dataset S1 shows sequencing statistics). As expected, H3K4me3 was particularly enriched at TSSs (*P* value < 1e-200 for each dataset).

To relate the genome-wide studies to our PCR-based results, we analyzed H3K4me3 occupancy around the *Bdnf* gene, including its TSSs, indicating that the H3K4me3 mark was present at the TSSs of *Bdnf* exons I–VII and absent at the coding exon. The ChIP-Seq data confirmed that the 12-wk-old R6/2 cortex showed lower H3K4me3 levels at the REST-regulated *Bdnf* exon II and within this exon, H3K4me3 occupancy was lost specifically at the RE-1 site for REST binding (Fig. 3*A*). We confirmed the ChIP-Seq results at other specific loci in cortex and striatum by ChIP-PCR; in the cortex, *Npas2* and *Npas4* had significantly lower levels of H3K4me3, and in the striatum, *Egr1* locus had significantly lower levels of H3K4me3 at TSS (Fig. S1 *G* and *H*).

Decreased H3K4me3 Occupancy Corresponds to Decreased Gene Expression Patterns. To identify genes that show significantly different levels of H3K4 trimethylation, we focused our analysis on a −3/+2-kb window around each TSS. We counted the number of reads in each of these windows and used loess normalization (*Materials and Methods*) to account for technical differences that might cause a systematic bias in the data between the R6/2 and WT mice, such as read complexity and genomic coverage. To integrate ChIP-Seq data with gene expression, RNA-Seq was performed on the same R6/2 and WT samples. Integration of ChIP-Seq and RNA-Seq results revealed a high degree of overlap between genes with decreased H3K4me3 (*Materials and*

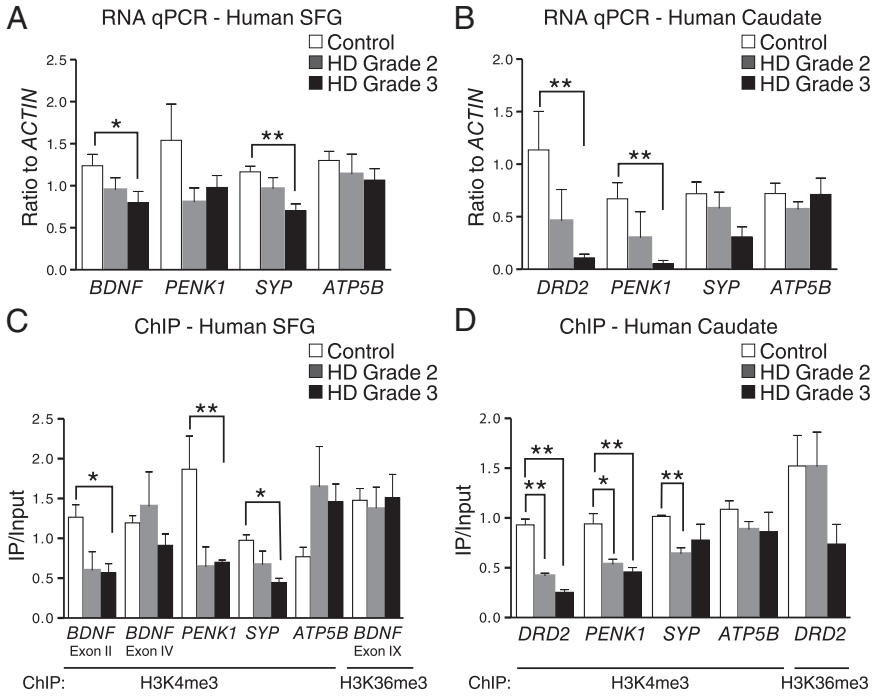

Fig. 2. H3K4me3 levels are selectively lower at promoters of down-regulated genes in human SFG and caudate. (*A*) *BDNF* and *SYP* gene expression was lower in grades 2 and 3 SFG samples compared with control SFG. For both genes, the difference between control and grade 3 samples was statistically significant (*BDNF* $P < 0.05$; *SYP* $P < 0.01$). *ATP5B* expression did not change, and *PENK1* expression was lower in both groups of HD tissues, although the difference did not achieve significance. (*B*) In the caudate, *DRD2* and *Penk1* expression was significantly lower in grade 3 patient samples ($P < 0.01$) than control levels. *ATP5B* expression did not change, and *SYP* expression showed trends in grades 2 and 3 samples, although the differences were not significant. (*C*) Levels of H3K4me3 at *BDNF* exon II are significantly lower in grade 3 SFG samples compared with control ($P < 0.05$), and they are not changed at exon IV promoter. Levels of H3K4me3 are also significantly lower at *PENK1* ($P < 0.01$) and *SYP* ($P < 0.05$) promoters in grade 3 SFG. H3K4me3 levels at *ATP5B* promoter and H3K36me3 levels at the *BDNF* coding region are not significantly different between control and grades 2 and 3 SFG. (*D*) In the caudate, H3K4me3 levels are significantly reduced at *DRD2* (grades 2 and 3; $P < 0.01$), *PENK1* (grades 2 and 3; $P < 0.05$ and $P < 0.01$, respectively), and *SYP* (grade 2; $P < 0.05$) promoters compared with control caudate samples. The *ATP5B* promoter showed no significant differences in H3K4me3 levels between control and HD samples. Although H3K36me3 levels at the *DRD2* coding region were lower than control caudate samples, the difference did not reach significance. For both caudate and SFG, four control samples were compared with three grade 2 and five to six grade 3 samples, and *t* tests were performed to calculate statistical significance. $*P < 0.05$; $**P < 0.01$.

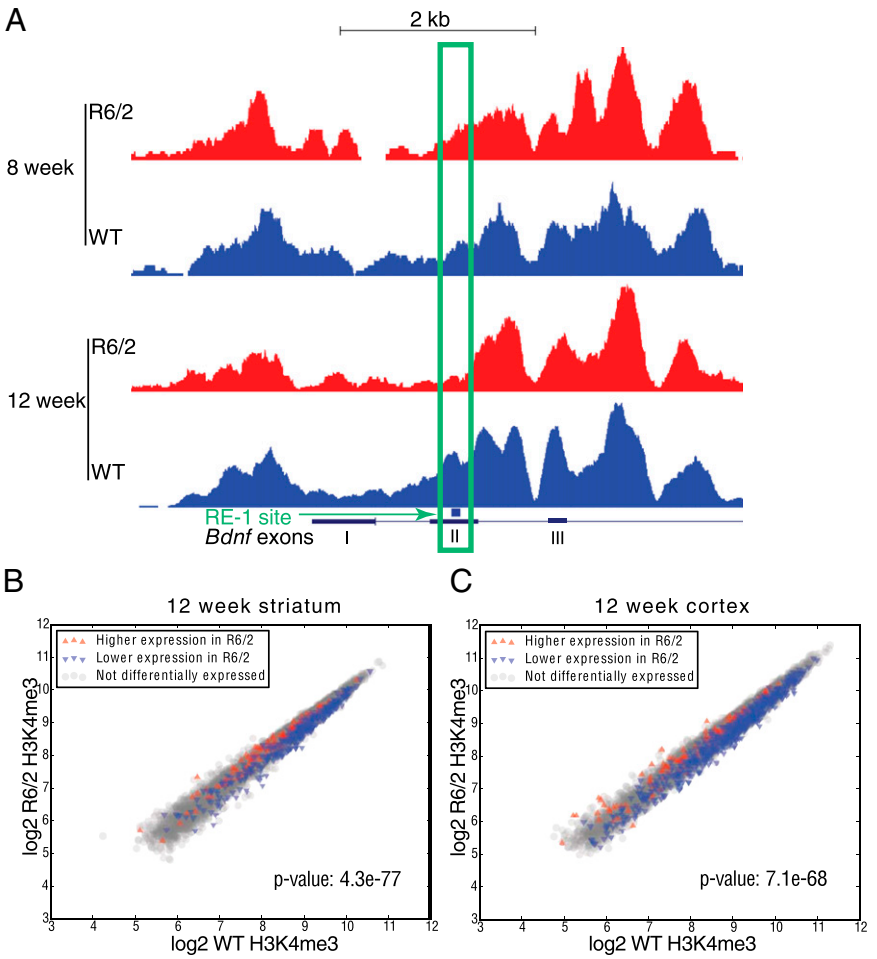

Fig. 3. H3K4me3 levels are lower at the REST-regulated *Bdnf* promoter in 12-wk-old R6/2 mouse cortex, and differentially expressed genes tend to show differential H3K4me3 in the striatum and cortex of R6/2 mouse at 12 wk of age. The plotted values represent the number of sequence reads at each position around the *Bdnf* locus after normalizing to the number of reads under all of the peaks in the same dataset, and the scale on the *y* axis is the same for R6/2 and WT. (*A*) This view is an expanded view of a 6-kb region centered on the REST binding site RE-1 in exon II. The top two tracks are from cortices of 8-wk-old mice, and the bottom two tracks are from cortices of 12-wk-old mice. The REST-regulated promoter of *Bdnf*, indicated by the green box, shows a significant difference between the animals at 12 wk, whereas this difference is not observed at 8 wk. Other regions of the gene are largely unchanged at either 8 or 12 wk of age. (*B* and *C*) Scatter plots for (*B*) 12-wk striatum and (*C*) 12-wk cortex show the extent of H3K4me3 signal detected in WT animals (*x* axis) vs. R6/2 animals (*y* axis) in a 2,000-bp window around the primary TSS of each gene with sufficient H3K4me3 coverage (*Materials and Methods*). The number of reads in each sample was transformed to $\log_2$ and normalized by loess regression. Genes that show higher expression in R6/2 mice (red) and genes with lower expression in R6/2 mice (blue) are indicated. Note that a large group of genes had both lower H3K4me3 (below the diagonal) and expression levels (blue) in R6/2 mouse (*C*) cortex and (*B*) striatum. *P* values represent the statistical significance of the overlap between genes down-regulated in R6/2 and genes with lower H3K4me3 levels, and they were computed using the hypergeometric distribution.

Methods) and decreased expression in R6/2 mice compared with WT mice at 8 and 12 wk in both cortex and striatum [hypergeometric *P* values: 8-wk cortex $P = 0.01$; 12-wk cortex $P =$ 7.1e-68; 8-wk striatum $P =$ 1.4e-5; 12-wk striatum $P =$ 4.3e-77 (Fig. 3 *B* and *C* and Fig. S2)] (Dataset S2 shows *P* values using a more stringent definition for decreased H3K4me3). Although there were fewer differentially expressed genes at 8 wk, an association between down-regulated gene expression and decreased H3K4me3 occupancy was still observed in R6/2 at this age (Fig. S2).

Transcriptome Analysis and Genome-Wide Analysis of H3K4me3 by ChIP-Seq in R6/2 Mouse Cortex and Striatum Reveals Alterations in Functionally Relevant Genes. We found the R6/2 transcriptome to be progressively and extensively dysregulated in both brain regions, consistent with previous reports using microarrays (12, 13). The most extensive dysregulation was observed in 12-wk cortex samples, where over 1,000 genes were differentially expressed under a false discovery rate of 10%. More than 600 genes were dysregulated in the 12-wk striatum. We compared our results with previous reports (22). Expression of representative dysregulated genes in these studies that are also dysregulated in our dataset is shown in Fig. 4. Fewer changes in gene expression were observed overall in 8-wk cortex and striatum compared with 12-wk cortex and striatum (170 and 134 genes for cortex and striatum, respectively). The majority of the dysregulated genes were down-regulated, especially for the 8-wk age. Gene expression tables for each region and age are in Dataset S3.

Similar to the transcriptome, differentially H3K4 trimethylated genes (1 SD from the regression line) (Fig. 3 *B* and *C*) were enriched for a number of gene ontology (GO) biological processes terms (Dataset S4), some of which were common in both cortex and striatum datasets. In 12-wk-old R6/2 mice, genes with reduced H3K4me3 were associated with terms that are highly relevant for brain physiological functions, such as synap-

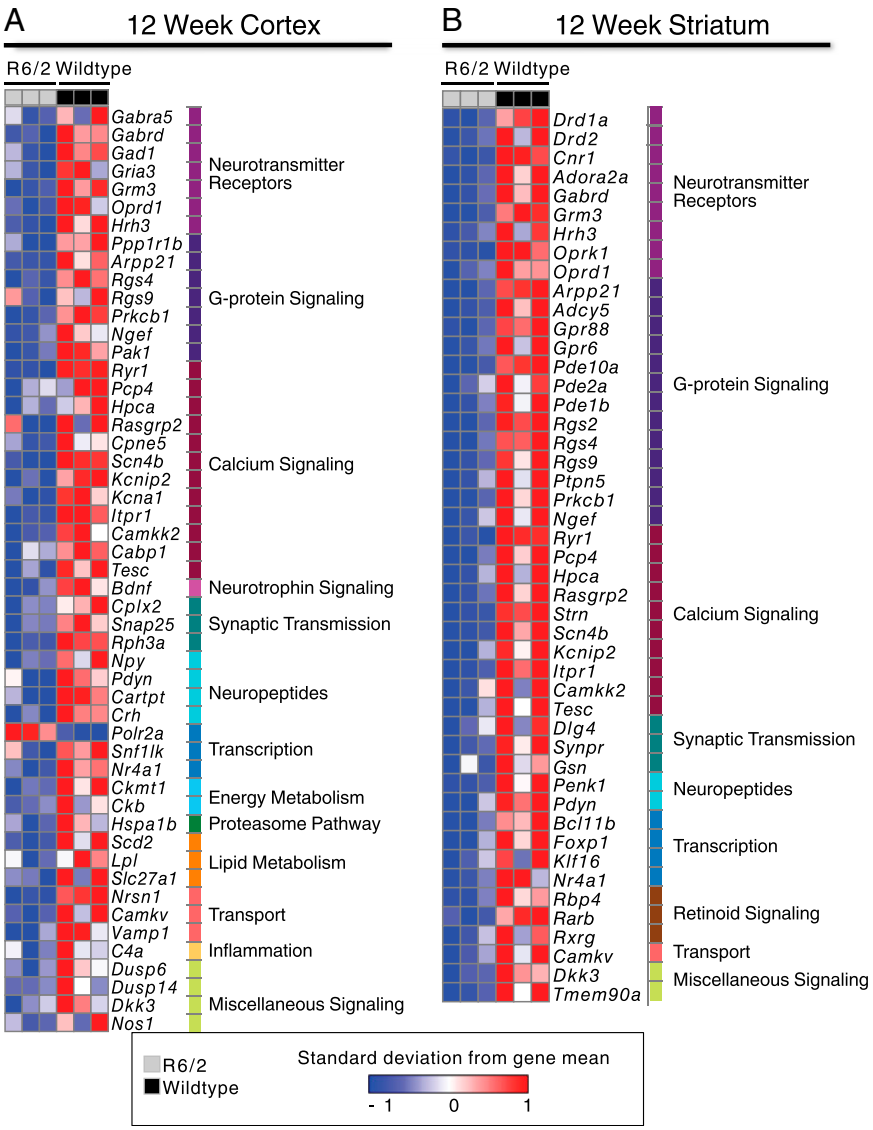

Fig. 4. Genes differentially expressed in R6/2 are representative of transcriptional dysregulation in HD. Heat maps of gene expression in 12-wk (*A*) cortex and (*B*) striatum for R6/2 ($n = 3$; gray) and WT littermates ($n = 3$; black). Previously identified HD-associated genes that were significantly differentially expressed in respective regions are shown. Reads per kilobase of exon model per million mapped reads values for each gene across all samples were mean-normalized and shown as ±1 SD. Of the genes shown in *A*, 41% also had significantly lower levels of H3K4me3 in R6/2. The corresponding number for *B* is 70%.

tic transmission, signal transduction, and G protein-coupled receptor signaling pathway. The list of genes with increased H3K4me3 was enriched for regulation of gene expression. In 8-wk-old R6/2 mice, similar overrepresented categories emerged. Biological processes, such as signal transduction, were overrepresented in the list of genes with lower H3K4me3 occupancy; processes, including RNA splicing and regulation of cell differentiation, were overrepresented among the set of genes with increased H3K4me3 occupancy (Dataset S4 shows complete lists of enriched GO terms).

In the 12-wk cortex, 293 down-regulated genes showed lower H3K4me3 levels at their promoters, including *Bdnf*, *Grin2c*, *Jun*, and *Arc*. Similarly, in the striatum of 12-wk-old R6/2 mice, 217 genes were down-regulated and showed reduction in H3K4me3 mark at their TSSs of greater than 1 SD from the loess regression line. It is noteworthy that 73 genes had lower levels of H3K4me3 and reduced expression in both the striatum and cortex of R6/2 mice at 12 wk of age, including activity-regulated genes, such as *Npas4* and *Arc*, as well as protein kinases, including *Camk4* and *Mapk4* (Dataset S2 shows the complete gene lists).

Down-Regulated Genes in R6/2 Mice Are Associated with a Specific H3K4me3 TSS Profile. Previous studies have shown that differences in the distribution of histone methylation around the TSS often distinguish classes of genes, even when these genes cannot be separated by their expression levels (23–26). Indeed, we observed an H3K4me3 profile in WT animals that distinguished between genes that decrease in expression in the mutant mice and genes that do not decrease. Specifically, in WT animals, there is a set of genes that has significantly higher levels of H3K4me3 in the coding regions compared with genes that are not differentially expressed in the mutants (Fig. S3 *A–D*). This pattern is exemplified by *Bdnf*, *Arc*, and *Grin2c* (Fig. 3*A* and Fig. S3*E*). By contrast, *Lin7c* and *Atp5b* are examples of genes that are not differentially expressed in the mutants and show similar levels of H3K4me3 levels around their TSSs in WT and mutant animals (Fig. S3*F*).

To investigate the H3K4me3 mark more rigorously, we used *k*-means clustering (*Materials and Methods*) to identify five predominant patterns of H3K4me3 that occur in both WT and R6/2 mice (Fig. 5 *A* and *B* for 12-wk cortex and striatum and Fig. S4 *A* and *B* for 8-wk cortex and striatum). Strikingly, there is a specific H3K4me3 profile in WT mice marking a very large fraction of genes that will be down-regulated in the presence of mutant HTT. In particular, genes down-regulated in R6/2 are very likely to be members of a particular cluster that we label as class 1, which has a broad peak of H3K4me3 downstream of the TSS in WT mice [*P* values: 12-wk cortex $P = 2.00e\text{-}59$; 8-wk cortex $P = 1.12e\text{-}16$; 12-wk striatum $P = 8.05e\text{-}38$; 8-wk striatum $P = 1.82e\text{-}9$ (Fig. 5 *A* and *B* and Fig. S4 *A* and *B*)]. Of 607 genes that are down-regulated in 12-wk cortex and have sufficient H3K4me3 coverage to be assigned a profile, 315 (52%) genes were in class 1 as opposed to 14%, 12%, 11%, and 10% in classes 2, 3, 4, and 5, respectively (Fig. 5 *C* and *D* and Fig. S4 *C* and *D*). This association strengthens from 8 to 12 wk of age as R6/2 mice progress through the pathological program caused by expression of the expanded CAG repeat in the *HTT* gene. Interestingly, genes in class 1 are enriched in GO biological processes critical for neuronal functions, such as signal transduction, G protein-coupled receptor signaling, neurogenesis, axon guidance, learning or memory, and regulation of transcription (Dataset S5). It is important to note that class 1 genes show similar expression levels to other classes (Fig. S4 *E–H*). Therefore, we conclude that this pattern cannot be explained as a simple consequence of differences in transcription.

Although the class 1 H3K4me3 profile in WT mice is strongly associated with down-regulation of expression of the corresponding genes in R6/2 animals, it is also important to note that, as the disease progresses, genes in the class 1 H3K4me3 group remain in that class. They do show a decrease in the levels of H3K4me3, but this mark remains spread across the coding region in a profile that is distinct from other classes. Unlike genes that were down-regulated, genes that were up-regulated in R6/2 mice did not show any significant association to a particular H3K4me3 TSS profile, except for an association between up-regulated genes in the 12-wk R6/2 cortex and class 4 profile ($P = 1.49e\text{-}4$).

Potential Regulators of Differential Trimethylation. We used sequence analysis to identify potential transcriptional regulators that could be recruiting methyltransferases and demethylases to differentially expressed genes in R6/2 mice. Previous studies (24, 27) have shown that the sites of such regulators should not be expected directly underneath the peaks of methylation. Therefore, we determined the location of chromatin accessible binding sites for regulatory proteins near the enriched H3K4me3 regions in WT and R6/2 mice based on an empirical spatial distribution derived from DNase-Seq and H3K4me3 ChIP-Seq data (Fig. S4 *I* and *J*). Applying this method to our H3K4me3 data from WT mice yielded a set of sequences that we searched for known DNA binding motifs (Dataset S6).

This analysis reveals several potential regulators that have been previously associated with HD. Genes down-regulated for both expression and H3K4me3 are associated with motifs for REST/NRSF (12-wk cortex $P = 2.52e\text{-}11$; 12-wk striatum $P = 2.67e\text{-}8$ (217 promoters)] and Sp1 binding motif (12-wk cortex $P = 1.55e\text{-}10$; 12-wk striatum $P = 9.85e\text{-}11$). These two motifs are also enriched in class 1 genes (REST/NRSF: cortex $P = 7.66e\text{-}54$; striatum $P = 8.09e\text{-}61$; Sp1: 8-wk striatum $P = 7.25e\text{-}18$; 12-wk cortex $P = 8.43e\text{-}21$; 12-wk striatum $P = 9.85e\text{-}11$). Both REST (28) and Sp1 (29, 30) have been previously linked to HD. In addition, our motif analysis suggests other possible regulators linked to down-regulation of expression and H3K4me3, including PPAR (reviewed in ref. 31) and p53 (32, 33).

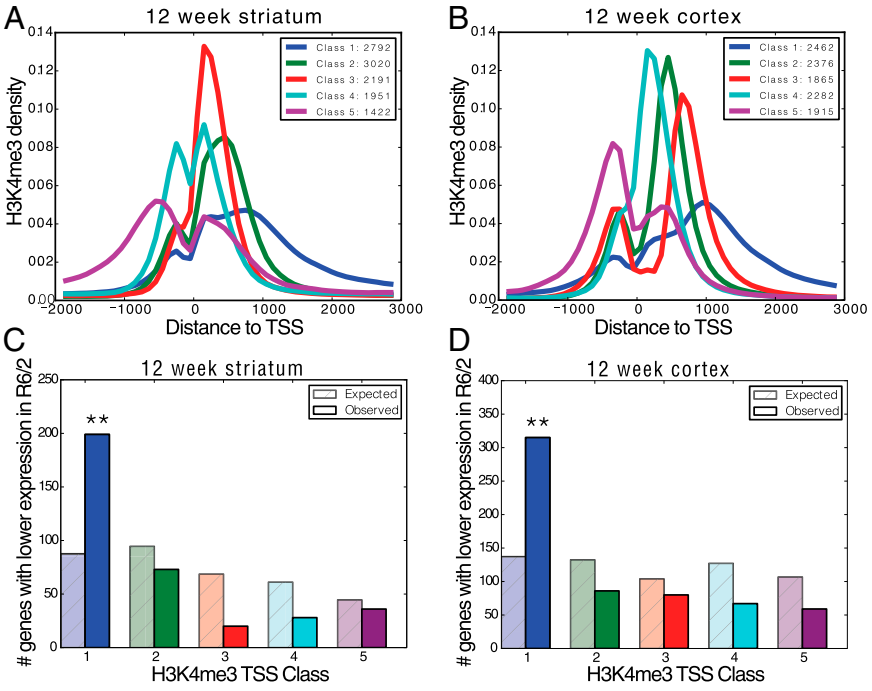

Fig. 5. Genes down-regulated in R6/2 mice have a distinct H3K4me3 profile in WT animals. Genes were clustered into five groups based on their H3K4me3 profiles in (*A*) striatum and (*B*) cortex of 12-wk-old WT animals. Plots show the density of sequence reads in window from −2 to +3 kb of the TSS. *A*, *Inset* and *B*, *Inset* show the numbers of genes in each class. Genes in class 1 (blue) show a broad peak of trimethylation starting at the TSS and extending into the coding region. In all datasets, this class is enriched in genes that are expressed at lower levels in R6/2. The numbers of genes with reduced expression expected and observed in each class are shown for (*C*) 12-wk striatum and (*D*) 12-wk cortex. $^{**}P < 0.01$.

Histone Demethylases Are Dysregulated in Mutant Htt-Expressing Brain Tissues. The identification of a specific signature of histone methylation associated with mutant HTT-induced pathology suggested the possibility that intervention designed to impact this methylation pattern could have significant therapeutic benefit in HD. To explore this approach for HD, we sought a strategy to manipulate histone methylation in a targeted manner. In our RNA-Seq data, five demethylases, including *Jarid1c*, *Jarid1b*, *Phf2*, *Mina*, *and Hspbap1*, showed a trend to increased expression in R6/2 brains (Fig. S5*A*), whereas there is no consistent down-regulation of histone methyltransferases (Fig. S5*B*). Among the histone demethylases, only *Jarid1b* and *Jarid1c* encode proteins with proven H3K4me3 demethylase activity (34). Although *Jarid1b* had slightly higher expression in WT brain, we focused on *Jarid1c*, which is relatively brain-enriched (35), is implicated in neuronal development (36), and had a stronger trend to dysregulation (Fig. S5*A*). More importantly, JARID1C interacts with REST (37), and the NRSE motif is strongly enriched near sites of reduced H3K4me3 (see above). *Jarid1c* was progressively dysregulated with expression similar between 4-wk-old WT and R6/2 mice, increased in R6/2 mice at 8 and 12 wk in cortex, and increased at 12 wk in striatum (Fig. S5*C*). Consistent with these studies in mice, *Jarid1c* was higher in grade 3 human HD caudate compared with control samples (Fig. S5*D*). These results are also consistent with findings that *Jarid1c* is increased in HD *Htt* (Q150) knockin mice (14).

***Jarid1c* Knockdown Reduces Toxicity and Modulates Mutant HTT-Mediated Transcriptional Dysregulation in Vitro and in Vivo.** First, we tested the effect of *Jarid1c* knockdown on primary cortical neurons (PCNs) derived from C57BL6 mice. Transduction of WT PCNs with lentiviruses expressing shRNA to *Jarid1c* resulted in >70% knockdown at the RNA level, with an apparent decrease of ∼50% at the protein level (Fig. S6*A*). Furthermore, knockdown resulted in increased BDNF protein levels determined by both ELISA and Western analysis (Fig. S6 *A* and *B*). In-cell Western analysis showed an enhancement in neurofilament (169 kDa) expression, which measures neuronal maturation (Fig. S6*C*), suggesting that knockdown improved the overall health of these neurons. We also found that knockdown of *Jarid1c* resulted in an increase in H3K4me3 levels at the REST-regulated exon II promoter of *Bdnf*, the REST-regulated *Synapsin I* and *Chrm4* promoters, and *Bdnf* exon IV, a non–REST-regulated promoter (Fig. S6*D*).

To test if modulation of *Jarid1c* activity counteracts the effects of mutant HTT, we evaluated the effects of acute *Jarid1c* knockdown in PCNs in the presence or absence of mutant HTT polypeptides. Primary cortical neurons were obtained from embronic day E16–E18 C57BL6 mouse embryos and cultured as described (38, 39) for up to 14 d. These neurons were transduced with lentivirus expressing GFP alone or the same region of mutant HTT encoded by exon 1 that is expressed in the R6/2 mice with 97 glutamines epitope tagged with GFP (97QP-GFP). In PCNs, by 4 d in vitro (DIV4), nuclear aggregates are visible in 97QP-GFP–expressing neurons. After 12 d in culture, cells expressing 97QP-GFP began to display reduced *Bdnf* and *Penk1* expression compared with cells transduced with GFP alone (Fig. 6*A*). We found that cotransduction with lentivirus expressing *Jarid1c* shRNA resulted in restoration of expression of these genes statistically similar to control GFP-expressing cells, whereas *Syp* expression increased above control levels (Fig. 6*A*). Interestingly, when we compared representative genes from various classes based on their H3K4me3 TSS profile in vivo, genes with the class I pattern were the most likely to decrease in expression with

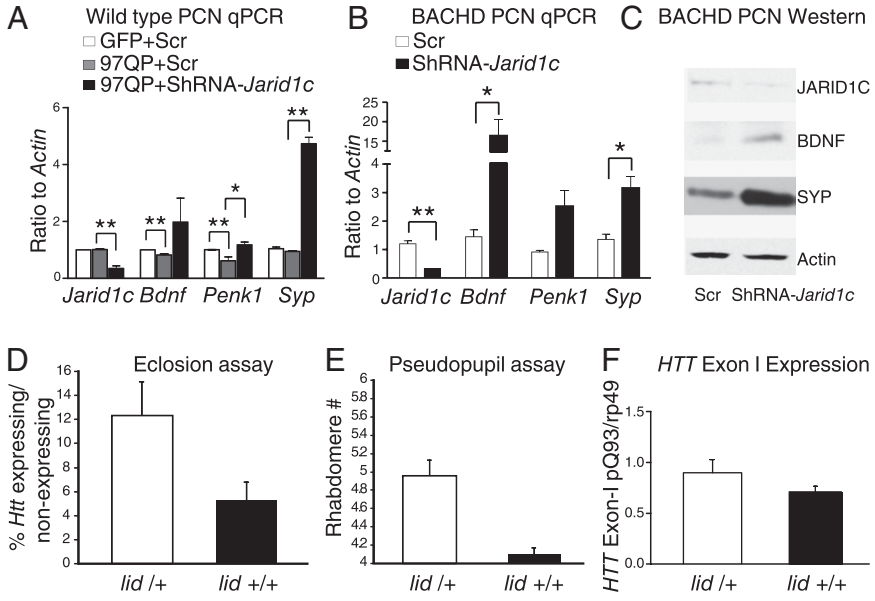

Fig. 6. Acute knockdown of *Jarid1C* prevents expanded HTT-mediated phenotypes. (*A*) Lentiviral-mediated expression of *HTT* exon I with expanded polyglutamines fused to GFP (97QP-GFP) in PCNs led to a decrease in expression of *Bdnf* and *Penk1* genes compared with *GFP* alone. This down-regulation was significantly reversed by knockdown of *Jarid1c*. *$P < 0.05$; $n = 3$. *Syp* expression was significantly increased on knockdown of *Jarid1c* ($P < 0.001$). (*B*) Knockdown of *Jarid1c* increased transcription of *Bdnf* ($P < 0.05$), *Penk1*, and *Syp* ($P < 0.05$) genes in primary cortical neurons cultured from BACHD neurons. (*C*) Western blotting shows that protein levels of SYP, a marker for synaptic health, as well as BDNF were increased in PCNs cultured from BACHD mice on acute knockdown of *Jarid1c*. (*D*) Reducing the dose of the demethylase *lid* leads to a significantly higher survival for flies with expanded polyglutamines. The eclosion rate of Htt-challenged flies that were also heterozygous for lid (lid/+) compared with $^{+/+}$ flies was improved ($P = 0.013$). Significance was measured by Student *t* test. (*E*) The effect of reduced levels of the demethylase lid on survival of photoreceptor neurons was evaluated by comparing the number of surviving photoreceptors in Htt-challenged animals with heterozygous siblings with one copy of the lid gene mutated. In this pseudopupil assay, reducing the dose of functional lid genes from two to one copy leads to a substantial improvement in photoreceptor neuron survival ($P = 0.0038$ comparing lid/+ with $^{+/+}$ flies). (*F*) Expression of the *HTT* exon 1 transgene was not altered in the crosses above as determined by qPCR. *$P < 0.05$; **$P < 0.01$.

97QP-GFP expression and increase in expression with *Jarid1C* knockdown (Fig. S6 *E* and *F*).

We next tested whether knockdown of *Jarid1c* could restore expression of *Bdnf* in PCNs derived directly from a full-length mutant HTT mouse model of HD. The BACHD mouse model (40) is a transgenic model expressing full-length mutant human *HTT* as a BAC transgene that begins to show symptoms beginning at 2–3 mo of age. The mice are visibly symptomatic by 10–12 mo of age, with dramatic brain weight and volume loss and protein aggregates. Reduction of *Jarid1c* after shRNA transduction into BACHD-derived PCNs was confirmed by quantitative PCR (qPCR) (Fig. 6*B*) and Western blot (Fig. 6*C*). Consistent with the findings above for WT neurons, a nearly fourfold increase in *Bdnf* is observed by Western blot analysis (Fig. 6*C*). These findings show that targeting this epigenetic mark increases expression of key genes in a full-length HD context. In both WT PCNs transduced with 97QP-GFP and BACHD neurons, knockdown of *Jarid1c* resulted in a large increase in expression of *Syp*, suggesting that the knockdown of *Jarid1c* may have generally neuroprotective properties in the presence of expanded polyglutamines (Fig. 6 *A*–*C*).

Finally, to assess whether the JARID1 class of demethylases might influence mutant HTT pathogenesis in vivo, we analyzed the effects of partial loss of its *Drosophila* single ortholog *little imaginal disks* (*lid*; CG9088), an H3K4me3-specific demethylase (41). In the *Drosophila* model used, the first exon of human *HTT* with an expanded polyglutamine domain (*HTTex1p-Q93*) is expressed in all neurons, resulting in reduced viability and progressive degeneration of neurons (42). *HTTex1p-Q93*–expressing flies that are either WT with two doses of *lid* or heterozygous for a mutation of *lid* (one dose) were compared with control siblings not expressing *HTTex1p-Q93*. Numbers of expanded repeat HTT-challenged flies surviving to adulthood (eclosing) when they had reduced *lid* (heterozygous for the lid^{10424} loss of function allele) were compared with flies homozygous for WT *lid*, and we found that, although the number of eclosed *HTTex1p-Q93* flies WT for *lid* was 5.3 ± 1.5% of nonexpressing control, the eclosion ratio of *HTTex1p-Q93* flies heterozygous for lid^{10424} increased to 12.4 ± 2.8% ($P = 0.013$, *t* test), suggesting neuroprotection (Fig. 6*D*). Neurodegeneration was analyzed by scoring the number of intact photoreceptor neurons in 7-d-old flies using the pseudopupil technique. When flies were reared at 22.5 °C and shifted to 25° C on eclosion, the average number of rhabdomeres (light-gathering structures of photoreceptor neurons) per ommatidium was 4.10 ± 0.07 in *HTTex1p-Q93*–expressing flies with WT *lid* ($^{+/+}$), whereas in *HTTex1p-Q93*–expressing flies with heterozygous lid^{10424} ($^{+/-}$), the average number of rhabdomeres increased to 4.96 ± 0.16 ($P = 0.0038$, *t* test) (Fig. 6*E*). Levels of the *HTT* transgene expression were not affected by heterozygosity for *lid* (Fig. 6*F*). Thus, our results indicate that reduced *lid* activity ameliorates mutant HTT-induced in vivo phenotypes in *Drosophila*.

Discussion

We find that expression of polyglutamine-expanded *HTT* is strongly associated with a specific pattern of histone methylation. Manipulation of histone methylation levels can at least partially restore transcriptional dysregulation in primary neurons and is neuroprotective in flies, suggesting that chromatin-modulating enzymes, including JARID1C, are rational therapeutic targets for HD treatment. Genes that decrease in expression in R6/2 mice because of the presence of a pathological *HTT* exon 1 transgene have an unusual pattern of H3K4me3, even in WT animals. This H3K4me3 pattern, which spreads broadly downstream of the TSS, is even associated with decreased expression of genes that maintain stable levels of H3K4me3 in 12-wk cortex ($P = 1.2e\text{-}13$) and striatum ($P = 1.7e\text{-}04$). These data suggest that the profile may be associated with recruitment of proteins with presence or absence in R6/2 that causes transcriptional dysregulation without changes in H3K4me3. We propose that this observation—genes that will be down-regulated in R6/2 animals have a specific distribution pattern of H3K4me3, even in striatal and cortical cells of normal animals—is an important clue to understanding the mechanistic basis of transcriptional dysregulation in HD.

The view that the distinctive architecture of H3K4 methylation at TSSs is a defining functional characteristic of classes of promoters is supported by observations in a wide range of eukaryotic systems. For example, in *Arabidopsis*, genes with expression patterns that are altered in response to dehydration show a pattern of H3K4me3 at transcriptional start sites similar to the one that we observe for down-regulated HD genes, and this pattern persists in both the dehydrated and watered state (26). The H3K4me3 classes that we observe also closely resemble the clusters previously reported for H3K4me2 in human CD4+ T cells (27). In this case, genes with tissue-specific expression showed a broader distribution of the mark extending into the expressed portion of the gene, suggesting that a unique chromatin signature at specific promoters may regulate their tissue-specific expression. Finally, there is precedence for specific classes of H3K4me3 profiles in brain that may be involved in tissue-specific expression, because five different classes of genes were identified in neurons isolated from prefrontal cortex, with genes encoding proteins with neuronal function having a similar broader distribution of H3K4me3 (43).

Considering these findings in diverse species together, we suggest that the observed H3K4me3 architecture reveals a fundamental property controlling expression levels, and in HD, it determines a response to *HTT* exon 1 expression. One important open question is how the pattern of H3K4me3 relates to other epigenetic features. Expression of mutant *HTT* has recently been shown to be associated with changes in DNA methylation (44), and there are precedents for a connection between changes in DNA methylation and trimethylation of H3K4 (45–47). We, therefore, propose that uncovering the regulatory mechanisms that establish, maintain, and respond to the characteristic epigenetic patterns at sensitive promoters, including the specific complexes formed and cross-talk between histone modifications and DNA modifications, should give insight into why these genes are particularly sensitive to the presence of mutant *HTT* and may provide insights into how to restore their transcription.

A key question that our studies raise is whether mutant HTT exerts its effects on down-regulated promoters through a direct and preferential action with chromatin at the site of each promoter or alternatively, mutant *HTT* acts to activate a cell signaling pathway that impacts H3K4me3 at target sites when activated by mutant HTT. Understanding which of these alternative mechanisms underlies the phenomena that we reported here will have impact on the strategy for additional development of therapeutic intervention for HD.

Materials and Methods

ChIP-PCR. Finely chopped pieces of one hemisphere of cortex or both halves of striatum were fixed with 1% formaldehyde at 37 °C for 15 min and then washed with ice-cold PBS two times. For human samples, ~100 mg tissue were finely chopped and fixed with 1% (vol/vol) formaldehyde. The fixed brain sections were prepared as described previously (48) and in *SI Materials and Methods*. Before addition of the H3K4me3 antibody for immunoprecipitation, 0.5% (vol/vol) of each sample was taken as input. The cross-links were reversed in the input samples, and after precipitation, DNA was resuspended in 20 μL deionized water. In the remaining sample, antibody was added and incubated overnight. After immunoprecipitation, washes, reversal of cross-links, and precipitation of DNA, the pellet was resuspended in 20 μL deionized water, and this sample was denoted as the IP sample. Gene-specific primers were used for qPCR (Dataset S7), and 1 μL input and IP samples were used in each PCR. The Δcrossing threshold (Ct) values between IP and input were compared among different samples.

ChIP-Seq Preparation and Analysis. Cortical and striatal tissues were cross-linked with 1% (vol/vol) formaldehyde for 10 min, and the cross-linking was quenched by 0.125 M final concentration glycine. The cross-linked tissue was then homogenized, rinsed with PBS, pelleted, and frozen in liquid nitrogen for later use. ChIP-Seq assays were performed as previously described (49). Details of the ChIP-Seq experiments and its computational analysis are described in *SI Materials and Methods*.

Clustering of Histone Methylation Patterns. To search for different patterns of histone methylation, we computed a binary vector representing whether one or more reads from the H3K4me3 ChIP-Seq experiment was detected at each base in a window −2/+3 kb around TSSs. These vectors were binned, normalized, and then clustered by the *k*-means algorithm for $k = 5$ using Euclidean distance and complete linkage.

RNA-Seq. The RNA-Seq protocol was adapted from a previously published protocol (50) using Invitrogen reagents unless noted otherwise. Details of the experimental procedures are provided in *SI Materials and Methods*. Reads were mapped to mm9 with the Bowtie alignment program with setting –Best (51). Differentially expressed genes were identified with the R package DESeq (52) using a 10% false discovery rate cutoff and $\log_2$ difference of 0.5 between WT and mutant conditions. Outliers were further excluded by restricting the residual variance quotients to less than 10. Heat maps were produced from reads per kilobase of exon model per million mapped reads values using GENE-E (Broad Institute; http://www.broadinstitute.org/cancer/software/GENE-E/).

Motif analysis is described in *SI Materials and Methods*. Primary cortical neuron culture from WT mice was produced by lentiviral preparation and transduction. WT primary cortical neurons were obtained from E16–E18 C57Bl6 mice using previously published protocols (38, 39). All procedures were performed under an Institutional Animal Care and Use Committee-approved protocol. Briefly, dissected tissue was dissociated with trypsin, triturated, plated in six-well plates coated with poly-D-lysine, and cultured in neurobasal supplemented with N2 and B27 (Invitrogen). Cells were plated at a density of 1×10^6 cells/mL and maintained in cultures until transduction. Lentiviral production is described in *SI Materials and Methods*. Samples were tested for expression of BDNF and Penk1 by RT-PCR and H3K4me3 occupancy at their promoters by ChIP followed by qPCR. Primer sequences are provided in Dataset S7.

BACHD Primary Cortical Neuron Culture. Postnatal day (P) P0–P3 neonates from BACHD mice maintained on the FVB/NJ background (Stock 001800; Jackson Laboratory) were used to generate primary cortical or striatal neurons as previously described (53). Cortical neurons from each pup were maintained separately to allow for genotype determination and cultured at 600,000 cells per well on a 24-well plate. At DIV3, neurons were transduced with shRNA or scramble control by adding 2.72 μL virus titered at 2.2 E6TU/μL (multiplicity of injection of 10), and 24 h later, the media were changed with half-conditioned media; 5 d posttransduction, neurons were harvested for additional processing.

Western Immunoblotting and ELISA in Primary Neurons. Western immunoblotting for BDNF measurements was performed as described previously (54), and details are provided in *SI Materials and Methods*. BDNF rabbit polyclonal antibody (sc-546) was from Santa Cruz Biotechnology.

In-Cell Western Assay. Primary cortical neurons were prepared as described above and plated at a density of 50,000 cells per well in poly-L-Lysine–coated 96-well plates from BD Biosciences. The cells were inoculated with scrambled or shRNA virus at an MOI of 20 on DIV1 and fixed with 1% (vol/vol) paraformaldehyde on DIV5–10. The protocol for in-cell Western assay was modified from the protocol by LiCOR Biosciences. Primary antibody for neurofilament 165 kDa (2H3) was from Developmental Studies Hybridoma Bank and used at a 1:1,000 dilution.

RNA Extraction and qPCR. Cell were lysed in TRIzol, and RNA was run through the Qiagen RNeasy column with on-column DNase I digestion. cDNA was prepared from up to 1 μg RNA using RT supermix from BioRad. The resulting cDNA was diluted 1:5 in water and used for qPCR by the SYBR green method (BioRad). Primer sequences are provided in Dataset S7. For human brain samples, RNA integrity was determined by running the samples on Agilent Bioanalyzer (Agilent Technologies), and an RNA integrity number of four was used a cutoff number.

***Drosophila* Experiments.** Details of the crosses, analysis of phenotypes, and qPCR analyses are described in *SI Materials and Methods*.

ACKNOWLEDGMENTS. We thank Dr. Jack Reidling for helpful reading of the manuscript. We also acknowledge generation of lentivirus from the University of California at Los Angeles vector core and early studies in *Drosophila* by J. Pallos. This work was supported by the University of California at San Francisco Medical Scientist Training Program (I.H.K.), National Institute of Health Grants 2R01 NS45491 (to S.F.), NS-45283 (to J.L.M. and L.M.T.), NS-52789 (to J.L.M. and L.M.T.), U01-NS063953 Subaward (to J.L.M. and L.M.T.), U54-CA112967 (to E.F.), R01-GM089903 (to E.F.), c NS072793 (to L.M.T.), PN2EY016525 (subawards to L.M.T. and D.E.H.), National Research Service Award Grant 1F31 NS077543, CHDI Foundation (J.L.M.), Huntington's Disease Society of America (J.L.M. and L.M.T.), and the Hereditary Disease Foundation (L.M.T.). Work in the laboratory of D.E.H. was supported by funds from the Hereditary Disease Foundation through the Leslie Gehry Brenner Award for Innovation in Science (to D.E.H.) and Koch Institute Support (Core) Grant P30-CA14051 from the National Cancer Institute. Support also included computing resources from National Science Foundation Grant DB1-0821391 and sequencing support from National Institutes of Health Grant P30-ES002109. This work was made possible, in part, by the availability of the Optical Biology Shared Resource of Cancer Center Support Grant CA-62203 at the University of California at Irvine, the Johns Hopkins Center Without Walls for Huntington's Disease, and the sequencing for RNA-Seq and ChIP-Seq performed at the Massachusetts Institute of Technology BioMicro Center.

1. The Huntington's Disease Collaborative Research Group (1993) A novel gene containing a trinucleotide repeat that is expanded and unstable on Huntington's disease chromosomes. *Cell* 72(6):971–983.
2. Walker FO (2007) Huntington's disease. *Lancet* 369(9557):218–228.
3. Cha JH (2000) Transcriptional dysregulation in Huntington's disease. *Trends Neurosci* 23(9):387–392.
4. Cha JH (2007) Transcriptional signatures in Huntington's disease. *Prog Neurobiol* 83(4):228–248.
5. Zuccato C, Cattaneo E (2007) Role of brain-derived neurotrophic factor in Huntington's disease. *Prog Neurobiol* 81(5–6):294–330.
6. Bernstein BE, et al. (2002) Methylation of histone H3 Lys 4 in coding regions of active genes. *Proc Natl Acad Sci USA* 99(13):8695–8700.
7. Santos-Rosa H, et al. (2002) Active genes are tri-methylated at K4 of histone H3. *Nature* 419(6905):407–411.
8. Kim TH, et al. (2005) A high-resolution map of active promoters in the human genome. *Nature* 436(7052):876–880.
9. Hunter RG, McCarthy KJ, Milne TA, Pfaff DW, McEwen BS (2009) Regulation of hippocampal H3 histone methylation by acute and chronic stress. *Proc Natl Acad Sci USA* 106(49):20912–20917.
10. Tsankova NM, et al. (2006) Sustained hippocampal chromatin regulation in a mouse model of depression and antidepressant action. *Nat Neurosci* 9(4):519–525.
11. Jiang Y, et al. (2008) Epigenetics in the nervous system. *J Neurosci* 28(46):11753–11759.
12. Gupta S, et al. (2010) Histone methylation regulates memory formation. *J Neurosci* 30(10):3589–3599.
13. Hodges A, et al. (2006) Regional and cellular gene expression changes in human Huntington's disease brain. *Hum Mol Genet* 15(6):965–977.
14. Kuhn A, et al. (2007) Mutant huntingtin's effects on striatal gene expression in mice recapitulate changes observed in human Huntington's disease brain and do not differ with mutant huntingtin length or wild-type huntingtin dosage. *Hum Mol Genet* 16(15):1845–1861.
15. Zuccato C, et al. (2001) Loss of huntingtin-mediated BDNF gene transcription in Huntington's disease. *Science* 293(5529):493–498.
16. Strand AD, et al. (2007) Expression profiling of Huntington's disease models suggests that brain-derived neurotrophic factor depletion plays a major role in striatal degeneration. *J Neurosci* 27(43):11758–11768.
17. Apostol BL, et al. (2008) CEP-1347 reduces mutant huntingtin-associated neurotoxicity and restores BDNF levels in R6/2 mice. *Mol Cell Neurosci* 39(1):8–20.
18. Duan W, et al. (2008) Sertraline slows disease progression and increases neurogenesis in N171-82Q mouse model of Huntington's disease. *Neurobiol Dis* 30(3):312–322.
19. Mangiarini L, et al. (1996) Exon 1 of the HD gene with an expanded CAG repeat is sufficient to cause a progressive neurological phenotype in transgenic mice. *Cell* 87(3):493–506.
20. Aid T, Kazantseva A, Piirsoo M, Palm K, Timmusk T (2007) Mouse and rat BDNF gene structure and expression revisited. *J Neurosci Res* 85(3):525–535.
21. Zuccato C, et al. (2008) Systematic assessment of BDNF and its receptor levels in human cortices affected by Huntington's disease. *Brain Pathol* 18(2):225–238.
22. Seredenina T, Luthi-Carter R (2012) What have we learned from gene expression profiles in Huntington's disease? *Neurobiol Dis* 45(1):83–98.
23. Young MD, et al. (2011) ChIP-seq analysis reveals distinct H3K27me3 profiles that correlate with transcriptional activity. *Nucleic Acids Res* 39(17):7415–7427.
24. Heintzman ND, et al. (2007) Distinct and predictive chromatin signatures of transcriptional promoters and enhancers in the human genome. *Nat Genet* 39(3):311–318.
25. Pekowska A, Benoukraf T, Ferrier P, Spicuglia S (2010) A unique H3K4me2 profile marks tissue-specific gene regulation. *Genome Res* 20(11):1493–1502.
26. van Dijk K, et al. (2010) Dynamic changes in genome-wide histone H3 lysine 4 methylation patterns in response to dehydration stress in Arabidopsis thaliana. *BMC Plant Biol* 10:238.

27. Shu W, Chen H, Bo X, Wang S (2011) Genome-wide analysis of the relationships between DNaseI HS, histone modifications and gene expression reveals distinct modes of chromatin domains. *Nucleic Acids Res* 39(17):7428–7443.
28. Zuccato C, et al. (2003) Huntingtin interacts with REST/NRSF to modulate the transcription of NRSE-controlled neuronal genes. *Nat Genet* 35(1):76–83.
29. Dunah AW, et al. (2002) Sp1 and TAFII130 transcriptional activity disrupted in early Huntington's disease. *Science* 296(5576):2238–2243.
30. Li SH, et al. (2002) Interaction of Huntington disease protein with transcriptional activator Sp1. *Mol Cell Biol* 22(5):1277–1287.
31. Jin YN, Johnson GV (2010) The interrelationship between mitochondrial dysfunction and transcriptional dysregulation in Huntington disease. *J Bioenerg Biomembr* 42(3): 199–205.
32. Bae BI, et al. (2005) p53 mediates cellular dysfunction and behavioral abnormalities in Huntington's disease. *Neuron* 47(1):29–41.
33. Steffan JS, et al. (2000) The Huntington's disease protein interacts with p53 and CREB-binding protein and represses transcription. *Proc Natl Acad Sci USA* 97(12):6763–6768.
34. Pedersen MT, Helin K (2010) Histone demethylases in development and disease. *Trends Cell Biol* 20(11):662–671.
35. Xu J, Deng X, Disteche CM (2008) Sex-specific expression of the X-linked histone demethylase gene Jarid1c in brain. *PLoS One* 3(7):e2553.
36. Iwase S, et al. (2007) The X-linked mental retardation gene SMCX/JARID1C defines a family of histone H3 lysine 4 demethylases. *Cell* 128(6):1077–1088.
37. Tahiliani M, et al. (2007) The histone H3K4 demethylase SMCX links REST target genes to X-linked mental retardation. *Nature* 447(7144):601–605.
38. Kaech S, Banker G (2006) Culturing hippocampal neurons. *Nat Protoc* 1(5):2406–2415.
39. Loo DT, et al. (1993) Apoptosis is induced by beta-amyloid in cultured central nervous system neurons. *Proc Natl Acad Sci USA* 90(17):7951–7955.
40. Gray M, et al. (2008) Full-length human mutant huntingtin with a stable polyglutamine repeat can elicit progressive and selective neuropathogenesis in BACHD mice. *J Neurosci* 28(24):6182–6195.
41. Lloret-Llinares M, Carré C, Vaquero A, de Olano N, Azorín F (2008) Characterization of Drosophila melanogaster JmjC+N histone demethylases. *Nucleic Acids Res* 36(9): 2852–2863.
42. Steffan JS, et al. (2001) Histone deacetylase inhibitors arrest polyglutamine-dependent neurodegeneration in Drosophila. *Nature* 413(6857):739–743.
43. Shulha HP, et al. (2012) Epigenetic signatures of autism: Trimethylated H3K4 landscapes in prefrontal neurons. *Arch Gen Psychiatry* 69(3):314–324.
44. Ng CW, et al. (2013) Extensive changes in DNA methylation are associated with expression of mutant huntingtin. *Proc Natl Acad Sci USA* 110(6):2354–2359.
45. Deaton AM, et al. (2011) Cell type-specific DNA methylation at intragenic CpG islands in the immune system. *Genome Res* 21(7):1074–1086.
46. Landan G, et al. (2012) Epigenetic polymorphism and the stochastic formation of differentially methylated regions in normal and cancerous tissues. *Nat Genet* 44(11): 1207–1214.
47. Balasubramanian D, et al. (2012) H3K4me3 inversely correlates with DNA methylation at a large class of non-CpG-island-containing start sites. *Genome Med* 4(5):47.
48. Sadri-Vakili G, et al. (2007) Histones associated with downregulated genes are hypo-acetylated in Huntington's disease models. *Hum Mol Genet* 16(11):1293–1306.
49. Macisaac KD, Fraenkel E (2010) Sequence analysis of chromatin immunoprecipitation data for transcription factors. *Methods Mol Biol* 674:179–193.
50. Levin JZ, et al. (2010) Comprehensive comparative analysis of strand-specific RNA sequencing methods. *Nat Methods* 7(9):709–715.
51. Langmead B (2010) Aligning short sequencing reads with Bowtie. *Curr Protoc Bioinformatics* 11(2010):11.7.
52. Anders S, Huber W (2010) Differential expression analysis for sequence count data. *Genome Biol* 11(10):R106.
53. Miller J, et al. (2011) Identifying polyglutamine protein species in situ that best predict neurodegeneration. *Nat Chem Biol* 7(12):925–934.
54. Lauterborn JC, et al. (2009) Ampakines cause sustained increases in brain-derived neurotrophic factor signaling at excitatory synapses without changes in AMPA receptor subunit expression. *Neuroscience* 159(1):283–295.
55. Pruunsild P, Kazantseva A, Aid T, Palm K, Timmusk T (2007) Dissecting the human BDNF locus: Bidirectional transcription, complex splicing, and multiple promoters. *Genomics* 90(3):397–406.